Astronomy & Astrophysics manuscript no. 8156
February 10, 2022
© ESO 2022

arXiv:0805.3399v1 [astro-ph] 22 May 2008

Galactic interstellar $^{18}O/^{17}O$ ratios - a radial gradient? ⋆

J.G.A. Wouterloot[1], C. Henkel[2], J. Brand[3], and G.R. Davis[1]

[1] Joint Astronomy Centre, 660 N. A'ohoku Place, Hilo, HI 96720, USA
[2] Max-Planck-Institut für Radioastronomie, Auf dem Hügel 69, 53121 Bonn, Germany
[3] INAF - Istituto di Radioastronomia, Via Gobetti 101, 40129 Bologna, Italy

Received date/ Accepted date

ABSTRACT

Context. The determination of interstellar abundances is essential for a better understanding of stellar nucleosynthesis and the "chemical" evolution of the Galaxy.
Aims. The aim is to determine $^{18}O/^{17}O$ abundance ratios across the entire Galaxy. These provide a measure of the amount of enrichment by high-mass versus intermediate-mass stars.
Methods. Such ratios, derived from the $C^{18}O$ and $C^{17}O$ J=1–0 lines alone, may be affected by systematic errors. Therefore, the $C^{18}O$ and $C^{17}O$ (1–0), (2–1), and (3–2), as well as the ^{13}CO(1–0) and (2–1) lines, were observed towards 18 prominent galactic targets (a total of 25 positions). The combined dataset was analysed with a large velocity gradient model, accounting for optical depth effects.
Results. The data cover galactocentric radii between 0.1 and 16.9 kpc (solar circle at 8.5 kpc). Near the centre of the Galaxy, $^{18}O/^{17}O$ = 2.88±0.11. For the galactic disc out to a galactocentric distance of ∼10 kpc, $^{18}O/^{17}O$ = 4.16±0.09. At ∼16.5 kpc from the galactic centre, $^{18}O/^{17}O$ = 5.03±0.46. Assuming that ^{18}O is synthesised predominantly in high-mass stars (M>8 $M_\odot$), while $C^{17}O$ is mainly a product of lower mass stars, the ratio from the inner Galaxy indicates a dominance of CNO-hydrogen burning products that is also apparent in the carbon and nitrogen isotope ratios. The high $^{18}O/^{17}O$ value of the solar system (5.5) relative to that of the ambient interstellar medium suggests contamination by nearby high-mass stars during its formation. The outer Galaxy poses a fundamental problem. High values in the metal-poor environment of the outer Galaxy are not matched by the low values observed towards the even more metal-poor Large Magellanic Cloud. Apparently, the outer Galaxy cannot be considered as an intermediate environment between the solar neighbourhood and the interstellar medium of small metal-poor galaxies. The apparent $^{18}O/^{17}O$ gradient along the galactic disc and the discrepancy between outer disc and LMC isotope ratios may be explained by different ages of the respective stellar populations. More data from the central and far outer parts of the Galaxy are, however, needed to improve the statistical significance of our results.

Key words. ISM: abundances – ISM: clouds – ISM: molecules – Galaxy: abundances – Radio lines: ISM – Nuclear reactions, nucleosynthesis, abundances

1. Introduction

Isotope abundance ratios play an important role in our understanding of stellar nucleosynthesis and the secular "chemical" enrichment of the interstellar medium by stellar ejecta. While isotope ratios are not easily measured at optical wavelengths, observations of molecular clouds with their large number of molecular species allow us to distinguish between various isotopic species. In principle, accurate line intensity- and abundance-ratios can then be determined.

A particularly useful tracer of nuclear processing and metal enrichment is the $^{18}O/^{17}O$ ratio because ^{18}O must be released primarily from high-mass stars (M>8$M_\odot$), while ^{17}O may predominantly be ejected from stars with lower mass (Henkel & Mauersberger 1993; Henkel et al. 1994; Langer & Henkel 1995). Heger & Langer (2000) concluded that at the surface of rotating stars with masses of 8–25$M_\odot$, ^{17}O is enriched and ^{18}O is depleted during hydrostatic burning prior to the supernova event. Most mass is ejected later, during the supernova explosion. While Hoffman et al. (2001) conclude that production of both ^{18}O and ^{17}O in massive stars is reduced when taking into account new nuclear reaction rates, these reaction rates remain uncertain (see e.g. Stoesz & Herwig 2003). To summarise, measured $^{18}O/^{17}O$ ratios have the potential to provide relevant constraints for models of stellar nucleosynthesis and "chemical" evolution.

The $^{18}O/^{17}O$ ratio is readily determined from the $C^{18}O/C^{17}O$ line intensity ratio. Both $C^{18}O$ and $C^{17}O$ have similar chemical and excitation properties. Rotational lines of both isotopologues are traditionally assumed to be optically thin, although $C^{18}O$ can reach considerable optical depths in some regions (e.g., Bensch et al. 2001). Oxygen isotopes are not fractionated (e.g., Langer et al. 1984), which is related to the high first ionization potential of oxygen, 13.6 eV. Thus, O^+ should have a low abundance in molecular clouds and charge exchange reactions like those for carbon (see Eq. 1 in Watson et al. 1976) should not significantly affect atomic and molecular oxygen abundance ratios. To summarise, observed CO line intensity ratios are a good measure of $^{18}O/^{17}O$.

Ratios of $^{18}O/^{17}O$ have commonly been determined for clouds in the solar neighbourhood and the inner Galaxy (see the reviews of Wilson & Matteucci 1992; Henkel et al. 1994; Wilson & Rood 1994; Kahane 1995; Bieging 1997). For the galactic disc and centre region, Penzias (1981) reported average $^{18}O/^{17}O$ ratios of 3.65±0.15 and 3.5±0.2, respectively. He found no significant gradient with galactocentric distance out to R_{GC}=10 kpc

Send offprint requests to: J.G.A. Wouterloot e-mail: j.wouterloot@jach.hawaii.edu
⋆ Figure A.1 (the spectra) is available in electronic form

($R_\odot$=8.5 kpc). The $^{18}O/^{17}O$ ratio from HCO^+ J=1–0 in Sgr B2 (3.1±0.6; Guélin et al. 1982) is within the errors consistent with the CO results for the galactic centre region. The observed interstellar ratios as well as many ratios from envelopes of late-type stars of intermediate mass (some of them with $^{18}O/^{17}O<1$; e.g. Kahane et al. 1992) differ significantly from the solar system $^{18}O/^{17}O$ ratio of 5.5, and Prantzos et al. (1996) even considered the possibility of measurement errors in the galactic data.

The above-mentioned $C^{18}O$ and $C^{17}O$ observations were made in the J=1–0 transitions alone, which is not sufficient when trying to account for radiative transfer effects. There exist also some J=2–1 data (e.g. Hofner et al. 2000; White & Sandell 1995), but these have been used to analyse $C^{18}O$ optical depths and column densities, rather than studying the isotope ratio itself. Bensch et al. (2001) observed the definitely optically thin $^{13}C^{18}O$ and $^{13}C^{17}O$ J=1–0 lines and derived 4.15±0.52 at one position in the nearby (d∼140 pc) ρ Oph cloud. The same cloud was observed towards 21 positions in the J=1–0, 2–1, and 3–2 transitions of $C^{18}O$ and $C^{17}O$ by Wouterloot et al. (2005). Large Velocity Gradient (LVG) model calculations combining these data resulted in a similar but more accurate value, 4.11±0.14, for the $^{18}O/^{17}O$ ratio. Very recently, Zhang et al. (2007) measured the J=1–0 lines towards a selected area of the southern star forming region NGC 6334 (d∼1.7 kpc). Under the (in this case realistic) assumption that all $C^{18}O$ lines were optically thin, they obtained a ratio of 4.13±0.13.

To date, little has been done to analyse molecular abundances in clouds at the edge of the Galaxy (for a pioneering study, see Wouterloot & Brand 1996). With respect to the solar neighbourhood, the far-outer Galaxy, at galactocentric radii of R_{GC}>16 kpc, is characterised by a low metallicity, a weak interstellar radiation field, a small cosmic ray flux, and a low large-scale average gas pressure (Brand & Wouterloot 1995, Ruffle et al. 2007, and references therein).

Our initial measurements of two objects at large galactocentric radii, DDT94 Cloud 1 and DDT94 Cloud 2 (Digel et al. 1994), with distances of R_{GC} of 22 and 17±2 kpc (Smartt et al. 1996) did not provide conclusive results. Therefore, to derive more reliable values, we have observed four objects from the catalogue of Wouterloot & Brand (1989) with stronger $C^{18}O$ lines (T_A^* ∼ 1 K versus 0.2 K for the DDT94 clouds) to cover the range of R_{GC} beyond 15 kpc. In addition, we have reobserved objects at 0 kpc ≲ R_{GC} ≲ 10 kpc to compare these results with previous estimates based on the J=1–0 line alone. Our sample consists of 25 positions in 18 sources that are observed in the J = 1–0, 2–1, and 3–2 rotational lines of $C^{18}O$ and $C^{17}O$. ^{13}CO(1–0) and (2–1) data were also taken.

2. Observations

2.1. IRAM 30-m

On March 4, 1995, we used the IRAM 30-m telescope[1] to observe $C^{18}O$ and $C^{17}O$ (1–0, 2–1) towards DDT94 Cloud 1 and 2. Between July 28 and August 2, 1995, we used the same telescope to observe $C^{18}O$ (1–0, 2–1) and $C^{17}O$ (1–0, 2–1) (see Table 1) towards the other clouds of our sample. We used three SIS receivers simultaneously (first for $C^{18}O$ J=1–0, 2–1 and $C^{17}O$ 2–1, then for $C^{17}O$ 1–0, 2–1 and $C^{18}O$ 2–1; all data were consistent) in combination with an autocorrelator split into three parts with equal velocity resolutions (in most cases 0.10 km s^{-1}).

[1] IRAM is supported by INSU/CNRS (France), the MPG (Germany), and the IGN (Spain).

Table 1. Observed transitions.

Molecule	Frequency (MHz)	HPBW[a] (arcsec)	B_{eff}^b	F_{eff}^b
$^{12}C^{18}O$(1–0)	109782.182	21	0.68	0.92 (1995,1996)
			0.76	0.92 (05-2000)
			0.76	0.92 (09-2000)
$^{12}C^{17}O$(1–0)	112359.277	21	0.68	0.92 (1995,1996)
^{13}CO(1–0)	110201.370	21	0.76	0.90 (05-2000)
			0.76	0.92 (09-2000)
$^{12}C^{18}O$(2–1)	219560.319	11	0.41	0.86 (1995,1996)
			0.54	0.91 (05-2000)
			0.54	0.85 (09-2000)
$^{12}C^{17}O$(2–1)	224714.370	11	0.41	0.86 (1995,1996)
^{13}CO(2–1)	220398.686	11	0.54	0.92 (05-2000)
			0.54	0.85 (09-2000)
$^{12}C^{18}O$(3–2)	329330.545	14	0.71	-
$^{12}C^{17}O$(3–2)	337061.129	14	0.71	-

[a]: Half Power Beam Width
[b]: Beam (B_{eff}) and forward hemisphere (F_{eff}) efficiency. To convert T_A^* antenna temperatures to T_{mb} main beam brightness temperatures, multiply the J=1–0 and 2–1 values by F_{eff}/B_{eff} (see, e.g., Rohlfs & Wilson 1996). For the J=3–2 lines, multiply by $1/B_{eff}$.

Towards most positions we initially used frequency-switching (by 7.9 and 15.8 MHz at 3 mm and 1.3 mm, respectively). Towards sources with broad lines, however, we observed in a position-switching (total power) mode. Offsets of the reference positions are given in Table 2. Velocity resolutions and rms values of the spectra are displayed in Table 3 (see Sect. 3). At positions with weak $C^{17}O$ lines, frequency-switched spectra showed prohibitively large baseline ripples. Therefore these sources were also observed in total power mode. From most spectra obtained in total power mode we subtracted a low order baseline. Remaining baseline ripples due to standing waves were removed by subtracting a sinusoidal baseline.

To investigate the importance of radiative transfer effects we observed ^{13}CO (1–0) and (2–1) simultaneously with $C^{18}O$ (1–0) and (2–1) between May 10 and 15 and on September 7, 2000. All observations were made in a total power mode. For the four sources from the sample of WB89, the ^{13}CO and $C^{18}O$ data were taken from Wouterloot & Brand (1996).

On April 4-5, 2005, we used HERA to observe $C^{18}O$ (2-1) towards all sources. HERA consists of two 9 pixel receivers on 3x3 arrays (a 24″ raster). The spectral resolution was 0.11 km/s and observations were made using position switching. These data are used to convolve the J=2–1 and J=3–2 spectra to the IRAM J=1–0 angular resolution.

An rms pointing accuracy of about 3″ was determined from scans across nearby continuum sources. Planet measurements showed that the receiver alignment was within 1–4″. The observed transitions, frequencies, beamsizes, beam and forward efficiencies are given in Table 1. In the following, T_A^* intensities are given, unless specified otherwise.

2.2. JCMT 15-m

On July 14, 2001, we observed $C^{17}O$(3–2) towards W49N and W51d with the 15-m James Clerk Maxwell Telescope

(JCMT)[2] using position switching. On various occasions between November 7, 2004, and May 19, 2005, we observed $C^{17}O$(3–2) towards NGC2024, L134N, and four offset positions near Ori-KL. $C^{18}O$(3–2) was observed towards the same sources and towards WB89-501. On February 10, 2006, we observed the remaining sources (except for the WB89 objects and G34.3+0.2, W3OH, and NGC7538) in $C^{18}O$ and $C^{17}O$(3–2).

The JCMT observations were made with the 2x800 channel DAS autocorrelator and the dual polarization RxB3 SIS receiver using position switching. The channel spacing was 156 – 625 kHz and the bandwidth was 250 – 920 MHz, depending on the line width of the source. Offsets of the reference positions used are given in Table 2. Pointing was done on nearby continuum sources and was generally accurate to within 3″.

From the JCMT archives we obtained $C^{17}O$(3–2) and $C^{18}O$(3–2) data towards G34.3+0.2, W3OH, and NGC7538. The JCMT archival data are from standard sources which are frequently observed, and always after doing a pointing observation on the source itself. The coordinates are within a few arcsec (much less than the beamsize and within the pointing accuracy) of the positions used for our IRAM 30-m observations. In some cases several spectra were available. Discrepant results and measurements with too low velocity resolution, affecting peak intensities, were not considered and the remaining spectra were averaged.

2.3. Calibration uncertainties

Calibration uncertainties in individual spectra may amount to ±10% which corresponds to ±14% in line intensity ratios. Changes in telescope efficiencies (see Table 1) may also contribute to the error budget. Like the uncertainties in the efficiencies, pointing errors may also affect those intensity ratios where the two lines were measured separately. This holds for all JCMT observations. As mentioned in Sect. 2.2, however, results from repeatedly observed sources turn out to be consistent. A direct way to assess the quality of the IRAM data is provided by Table 3. Here, line parameters for the $C^{18}O$ J=1–0 and 2–1 lines are given twice, because the lines were once observed together with $C^{17}O$ and another time with ^{13}CO. The uncertainty in the IRAM line ratios will be less than those in the line intensities which are suggested by differences between both sets of $C^{18}O$ measurements, because the ratios are commonly based on simultaneous observations. Nevertheless, the data displayed in Table 3 provide firm upper limits to the full error budget of the IRAM line intensities.

3. Results

Table 2 contains the sample of observed sources. Sgr B2 is the most prominent star-forming region close to the galactic centre, L 134N is a dark cloud near the Sun, and WB89 380, WB89 391, WB89 437, and WB89 501 are sources located in the far outer Galaxy. The other targets are star forming regions located at an intermediate range of galactocentric radii, extending from the inner "molecular ring" out to the Perseus arm.

[2] The JCMT is operated by The Joint Astronomy Centre on behalf of the Science and Technology Facilities Council of the United Kingdom, the Netherlands Organisation for Scientific Research, and the National Research Council of Canada. Our programs: m04bd10 and m05bi17. JCMT archive data were obtained from the Canadian Astronomy Data Centre, which is operated by the Herzberg Institute of Astrophysics, National Research Council of Canada.

The complete set of spectra is displayed in the appendix (Fig. A.1) that is available in electronic form. All spectra of an individual source are plotted on the same velocity scale. Line parameters obtained from Gaussian fits to the J=1–0, 2–1, and 3–2 transitions are summarised in Table 3. To compare abundances and not line intensities, we corrected the $C^{18}O/C^{17}O$ line intensity ratios for the difference in frequency of both isotopologues, following Linke et al. (1977) and Penzias (1981). This implies an increase of the ratios by a factor 1.047. For W51d, all parameters were calculated for two velocity intervals, accounting for the two emission lines at +50 and +60 km s^{-1} detected towards this source. The new $C^{18}O$ HERA line parameters towards the WB89 sources agree with those obtained earlier, also with the 30-m telescope, by Wouterloot & Brand (1996).

The resulting $C^{18}O/C^{17}O$ abundance ratios as a function of distance from the galactic centre, R_{GC} are shown in Fig. 1. Error bars accounting for the uncertainty in the line areas (obtained from baseline fits and given in Table 3), are not plotted to avoid confusion. For comparison we also show the results from Penzias (1981) for the J=1–0 transition. For the J=2–1 lines, we plot results from Hofner et al. (2000), who used the 30-m telescope to observe $C^{18}O$ and $C^{17}O$ towards HII regions of the inner Galaxy as well as towards W3(OH). The good agreement between our results and those of Penzias (1981) and Hofner et al. (2000) indicates that the calibration of our data is correct.

The distance to a given source can lead to a number of observational biases that are difficult to quantify and that do not facilitate a comparison between different parts of the Galaxy. With increasing distance, the linear beam size increases, leading potentially to the inclusion of a significant amount of relatively diffuse optically thin gas. On the other hand, a tendency to include brighter and more massive sources at larger distances may involve sources with systematically higher $C^{18}O$ opacities that may lead to underestimates of the $C^{18}O/C^{17}O$ abundance ratios. To search for a distance-related bias, Fig. 2 therefore shows the $C^{18}O/C^{17}O$ ratios as a function of solar distance d. In Fig. 3 we show the same as in Fig. 1, but for the ^{13}CO to $C^{18}O$ ratios obtained from the J=1–0 and 2–1 lines. In addition, Figs. 3c and d show correlations between the $^{13}CO/C^{18}O$ and $C^{18}O/C^{17}O$ ratios.

4. Discussion

4.1. Overall trends

Not accounting for optical depth effects and omitting Sgr B2 and the far outer Galaxy clouds, our average $C^{18}O/C^{17}O$ abundance ratios are 3.76±0.16 (J=1–0), 3.65±0.16 (J=2–1), and 3.08±0.12 (J=3–2), which can be compared with the Penzias (1981) J=1–0 galactic disc value of 3.65±0.15. The J=1–0 results agree within the errors. If we weight our data with their uncertainties, the average ratios become slightly smaller, i.e. 3.68±0.11, 3.38±0.13, and 2.74±0.10, respectively. We note, however, that smaller values tend to have smaller errors. Therefore, weighted averages may yield too small values and unweighted averages should be preferred. For the two SgrB2 positions average ratios are 2.99±0.06 (1–0), 2.26±0.17 (2–1), and 2.47±0.38 (3–2) (weighted 2.99±0.05, 2.27±0.14, and 2.32±0.30). The average ratios of the four far outer Galaxy clouds are 5.18±0.96 (1–0) and 5.02±0.22 (2–1) (weighted: 4.79±0.77 and 4.96±0.23).

Assuming that the $C^{18}O$ and $C^{17}O$ rotational lines are optically thin, the most important results that can be derived from Figs. 1 and 2 are: (1) *Our $C^{18}O/C^{17}O$ abundance ratios of the*

Table 2. Observed sources[a].

Source	α(2000) h m s	δ(2000) ° ′ ″	off α ″	off δ ″	ref α ′	ref δ ′	d kpc	R_{GC} kpc	ref
WB89 380	01 07 51.3	+65 21 25	0	0	1.2	16.7	10.4	16.8	(1)
WB89 391	01 19 25.4	+65 45 50	0	0	1.2	16.7	10.4	16.9	(1)
					−60	0			
DDT94 Cloud 1	02 04 51.9	+63 07 41	0	0			16.4	22.9	(2)
W 3	02 25 44.2	+62 06 01	0	0			2.0	10.0	(3)
W 3OH	02 27 04.2	+61 52 25	0	0	−60	0	2.0	10.0	(3)
					120	0			
WB89 437	02 43 29.0	+62 57 16	0	0	−13.7	6.2	9.1	16.2	(1)
					54.8	−24.8			
DDT94 Cloud 2	02 48 30.4	+58 27 47	0	0			10.0	17.0	(4)
WB89 501	03 52 27.7	+57 48 26	0	0	−11	9	8.6	16.3	(1)
					12.2	−10			
Ori KL	05 35 14.2	−05 22 26	0	0	−30	0	0.41	8.84	(5)
					45	0			
			30	−240					
			30	30					
			0	−150					
NGC 2024	05 41 45.4	−01 54 47	0	0	15	0	0.42	8.86	(6)
					30	0			
					−30	0			
L 134N	15 54 06.6	−02 52 19	−84	−48	20	10	0.11	8.41	(7)
Sgr B2(M)	17 47 20.4	−28 23 02	0	0	−30	60	8.5	0.1	(8)
			0	15	−30	60	8.5	0.1	
W 33	18 14 14.4	−17 55 50	0	0	−30	30	3.8	4.8	(2)
			0	24					
G34.3+0.2	18 53 18.4	+01 14 56	0	0	−30	30	3.9	5.7	(2)
W 49N	19 10 13.4	+09 06 14	0	0	0	−60	11.4	7.8	(9)
W 51d	19 23 39.6	+14 31 13	0	0	0	−60	7.0	6.6	(10)
DR 21	20 38 54.6	+42 19 23	0	0			2.0	8.5	(11)
DR 21cal	20 39 01.2	+42 19 45	0	0			2.0	8.5	(11)
DR 21OH	20 39 01.9	+42 22 46	0	0			2.0	8.5	(11)
NGC 7538	23 13 45.2	+61 28 10	0	0	0	−60	2.7	9.8	(12)
					0	60			

(1) Brand & Wouterloot (1994); peak position from Wouterloot & Brand (1996).
(2) Kinematic distance from the observed radial velocity and the rotation curve of Brand & Blitz (1993). For W33 and G34.3+0.2, the near kinematic distance is given.
(3) Weighted average of distances of Hachisuka et al. (2006), 2.04±0.07 kpc, Xu et al. (2006), 1.95±0.04 kpc, and Imai et al. (2000), 1.83±0.14 kpc.
(4) Smartt et al. (1996).
(5) Menten et al. (2007).
(6) Anthony-Twarog (1982).
(7) Franco (1989).
(8) Kerr & Lynden-Bell (1986); we note that Eisenhauer et al. (2005) derived 7.62±0.32 kpc for the distance to the Galactic Centre which may be compared with the IAU value of 8.5 kpc assumed in this work.
(9) Gwinn et al.(1992).
(10) Lacy et al. (2007).
(11) Dickel et al. (1978). DR 21cal position from Mauersberger et al. (1989).
(12) From trigonometric parallax of CH_3OH masers, L. Moscadelli pers. comm.
[a]: Source names (Col. 1); Source positions in equatorial coordinates (Cols. 2 and 3); Observed offset positions (Cols. 4 and 5); Offsets of the reference positions used for total power measurements (Cols. 6 and 7); Adopted distances from the Sun and the galactic centre (Cols. 8 and 9); Reference to these values (Col. 10).

inner galactic disc are consistent with those of Penzias (1981), while the ratios from the galactic centre region are smaller. (2) *There probably is a gradient with increasing $^{18}O/^{17}O$ ratios as a function of R_{GC} out to galactocentric distances of 16 kpc*. (3) *The solar system value is significantly larger than the ratios from the inner Galaxy, but not much higher than those from the far outer Galaxy*. (4) *An observational bias due to distance related effects is not apparent*.

Fig. 1a shows an increasing scatter in the J=1–0 ratios as a function of R_{GC}. While in the inner Galaxy ratios are $\lesssim$4, there are a few higher ratios observed in clouds near the solar circle. Two (50%) of the four far outer Galaxy (FOG) clouds are also characterised by a high ratio. The J=2–1 ratios show a more systematic increase with R_{GC} from about two near the galactic centre to about five at R_{GC}=16 kpc. The J=3–2 ratios may follow this trend, but the ratios are generally smaller. The different behaviour of the J=1−0, 2−1, and 3−2 transitions may

Table 3. Observed line parameters[a].

Source	rms	I	rms	I	rms	I	rms	I	rms	I	rms	I	(1–0)	(2–1)	(3–2)	rms	I	rms	I	rms	I	rms	I	(1–0)	(2–1)
($\Delta\alpha$,$\Delta\delta$)	dv	δI	dv	δI	dv	δI	dv	δI	dv	δI	dv	δI				dv	δI	dv	δI	dv	δI				
	(K and K km s^{-1})															(K and K km s^{-1})									
(arcsec)	(km s^{-1} and K km s^{-1})															(km s^{-1} and K km s^{-1})									
	C^{18}O(1–0)		C^{18}O(2–1)		C^{18}O(3–2)		C^{17}O(1–0)		C^{17}O(2–1)		C^{17}O(3–2)		C^{18}O/C^{17}O			^{13}CO(1–0)		^{13}CO(2–1)		C^{18}O(1–0)		C^{18}O(2–1)		^{13}CO/C^{18}O	
(1)	(2)	(3)	(4)	(5)	(6)	(7)	(8)	(9)	(10)	(11)	(12)	(13)	(14)	(15)	(16)	(17)	(18)	(19)	(20)	(21)	(22)	(23)	(24)	(25)	(26)
WB89 380	0.058	0.99	0.016	2.89			0.022	0.29	0.019	0.57			3.57	5.31		0.021	14.7	0.151	20.8	0.024	1.27	0.022	2.79	11.6	7.46
(0,0)	0.107	0.07	0.107	0.02			0.104	0.02	0.104	0.02			0.36	0.19		0.106	0.02	0.136	0.19	0.107	0.03	0.107	0.02	0.3	0.09
WB89 391	0.072	0.58	0.015	1.60			0.012	0.078	0.016	0.31			7.78	5.40		0.023	7.63	0.124	10.3	0.018	0.61	0.018	1.45	12.5	7.10
(0,0)	0.107	0.07	0.107	0.01			0.104	0.012	0.104	0.01			1.52	0.18		0.106	0.02	0.136	0.13	0.107	0.02	0.107	0.02	0.2	0.13
DDT94 Cloud 1	0.018	0.20	0.024	0.15			0.050		0.040				>1.75	>2.08												
(120,–170)	0.107	0.01	0.107	0.01			0.104		0.104				(3σ)	(3σ)												
W 3	0.058	3.26	0.075	7.07					0.076	2.02	0.052	2.31		3.66		0.054	54.3	0.174	86.7	0.065	3.76	0.118	9.18	14.4	9.44
(0,0)	0.107	0.07	0.107	0.09					0.104	0.09	0.556	0.15		0.17		0.272	0.12	0.425	0.47	0.273	0.12	0.427	0.29	0.5	0.30
W 3OH	0.064	11.8	0.041	20.3	0.051	40.2	0.041	3.19	0.034	6.06	0.058	14.7	3.87	3.51	2.86	0.051	75.8	0.081	85.0	0.048	11.8	0.071	27.2	6.42	3.13
(0,0)	0.107	0.10	0.107	0.08	0.284	0.14	0.104	0.07	0.104	0.05	0.279	0.15	0.09	0.03	0.03	0.272	0.13	0.425	0.29	0.273	0.13	0.427	0.23	0.07	0.03
WB89 437	0.049	1.68	0.015	2.86			0.019	0.30	0.013	0.69			5.86	4.34		0.028	15.2	0.079	15.4	0.023	1.44	0.026	3.12	10.6	4.94
(0,0)	0.107	0.06	0.107	0.02			0.104	0.02	0.104	0.02			0.38	0.14		0.106	0.04	0.136	0.11	0.107	0.03	0.107	0.03	0.2	0.05
DDT94 Cloud 2	0.016	0.14	0.024	0.20			0.028		0.019				>2.22	>6.06												
(50,35)	0.107	0.01	0.107	0.01			0.104		0.104				(3σ)	(3σ)												
WB89 501	0.043	0.57	0.016	1.83	0.130	2.37	0.022	0.17	0.019	0.38	0.039		3.51	5.04	>5.95	0.024	11.5	0.182	16.0	0.022	0.75	0.027	1.69	15.3	9.47
(0,0)	0.107	0.05	0.107	0.02	0.142	0.17	0.104	0.02	0.104	0.02	0.139		0.52	0.27	(3σ)	0.106	0.03	0.136	0.23	0.107	0.02	0.107	0.03	0.4	0.22
Ori KL	0.120	13.8	0.159	47.1	0.210	127	0.117	2.52	0.160	8.58	0.099	53.5	5.73	5.75	2.49	0.143	144.7	0.403	598.4	0.048	15.5	0.190	70.9	9.34	8.44
(0,0)	0.107	0.23	0.107	0.31	0.285	0.7	0.104	0.15	0.104	0.18	0.278	0.28	0.35	0.13	0.02	0.272	0.4	0.425	1.8	0.273	0.15	0.427	0.72	0.09	0.09
Ori KL	0.242	5.16	0.098	11.6	0.186	16.9	0.090	1.70	0.083	3.10	0.090	5.07	3.18	3.92	3.49	0.074	63.4	0.108	96.8	0.072	5.52	0.113	13.2	11.5	7.33
(30,−240)	0.107	0.25	0.107	0.10	0.285	0.31	0.104	0.09	0.104	0.08	0.278	0.15	0.23	0.10	0.12	0.272	0.12	0.425	0.23	0.273	0.09	0.427	0.23	0.2	0.13
Ori KL	0.237	10.4	0.252	19.3	0.207	35.3	0.146	3.25	0.117	5.96	0.096	12.6	3.35	3.39	2.89	0.056	79.2	0.111	154.9	0.068	11.7	0.107	32.5	6.76	4.77
(30,30)	0.107	0.25	0.107	0.26	0.285	0.35	0.104	0.15	0.104	0.12	0.278	0.16	0.17	0.09	0.05	0.272	0.09	0.425	0.2	0.273	0.11	0.427	0.22	0.06	0.03
Ori KL	0.239	3.54	0.074	10.5	0.200	18.4	0.071	1.20	0.055	2.88	0.093	5.92	3.09	3.82	3.25	0.079	40.2	0.109	75.1	0.074	4.80	0.104	12.7	8.38	5.91
(0,−150)	0.107	0.28	0.107	0.09	0.285	0.38	0.104	0.08	0.104	0.07	0.278	0.16	0.32	0.08	0.10	0.272	0.13	0.425	0.22	0.273	0.14	0.427	0.21	0.25	0.10
NGC 2024	0.134	7.45	0.061	13.1	0.222	14.2	0.080	2.06	0.054	3.55	0.092	4.09	3.79	3.86	3.63	0.072	55.8	0.092	60.4	0.059	6.74	0.099	12.0	8.28	5.03
(0,0)	0.107	0.13	0.107	0.06	0.285	0.37	0.104	0.08	0.104	0.06	0.278	0.15	0.16	0.06	0.16	0.272	0.072	0.425	0.19	0.273	0.09	0.427	0.19	0.12	0.08
L 134N			0.038	1.29	0.078	0.340	0.029	0.46	0.025	0.44	0.015	0.095	3.71[b]	3.07	3.75	0.167	6.82	0.122	4.19	0.190	1.64	0.114	1.40	4.15	2.99
(−84,−48)			0.053	0.02	0.142	0.038	0.052	0.02	0.052	0.02	0.139	0.006	0.27	0.15	0.48	0.027	0.06	0.136	0.09	0.027	0.07	0.137	0.08	0.18	0.19
Sgr B2(M)	0.160	96.7	0.196	136.3	0.101	263.2	0.089	33.1	0.166	58.1	0.074	136.7	3.06	2.46	2.02	0.045	487.8	0.255	627.9	0.040	111.4	0.098	277.6	4.38	2.26
(0,0)	0.107	0.47	0.107	0.58	0.569	0.7	0.208	0.26	0.104	0.49	0.556	0.5	0.03	0.02	0.01	2.72	0.7	0.425	1.7	2.73	0.6	0.427	0.6	0.02	0.01
Sgr B2(M)	0.118	64.9	0.163	72.6	0.102	192.3	0.071	23.2	0.114	36.6	0.079	69.0	2.93	2.07	2.92	0.037	399.9	0.213	363.7	0.024	77.4	0.092	101.0	5.17	3.60
(0,15)	0.107	0.33	0.107	0.44	0.569	0.6	0.208	0.19	0.104	0.30	0.556	0.49	0.03	0.02	0.02	2.72	0.4	0.425	1.4	2.73	0.33	0.427	0.5	0.02	0.02
W 33			0.229	46.1	0.087	76.0	0.257	11.5	0.173	14.8	0.061	32.8	3.98[b]	3.26	2.43	0.148	163.5	0.441	176.5	0.123	43.7	0.217	84.1	3.74	2.10
(0,0)			0.107	0.34	0.285	0.21	0.104	0.38	0.104	0.25	0.278	0.15	0.17	0.06	0.01	0.213	0.3	0.425	1.2	0.213	0.24	0.427	0.60	0.02	0.02
W 33	0.111	50.4	0.093	67.6	0.086	91.6	0.063	14.5	0.052	24.4	0.064	40.3	3.64	2.99	2.38	0.162	169.0	0.292	171.1	0.123	48.1	0.278	84.9	3.51	2.02
(0,24)	0.107	0.16	0.107	0.14	0.285	0.21	0.104	0.09	0.104	0.07	0.278	0.02	0.02	0.01	0.01	0.213	0.3	0.425	0.8	0.213	0.24	0.427	0.77	0.02	0.02
G34.3+0.2	0.090	40.2	0.144	63.4	0.061	101.2	0.169	10.8	0.176	26.1	0.049	41.1	3.89	2.54	2.58	0.175	118.3	0.257	150.9	0.116	42.2	0.284	87.0	2.80	1.73
(0,0)	0.107	0.13	0.107	0.15	0.569	0.2	0.104	0.20	0.104	0.26	0.556	0.14	0.07	0.03	0.01	0.213	0.4	0.425	0.8	0.213	0.24	0.427	0.83	0.02	0.02
W 49	0.154	38.9	0.175	90.2	0.077	163.1	0.079	11.0	0.092	22.0	0.064	53.6	3.70	4.29	3.19	0.139	240.4	0.224	436.8	0.107	38.1	0.263	103.6	6.31	4.22
(0,0)	0.107	0.35	0.107	0.39	0.569	0.4	0.208	0.18	0.104	0.21	0.278	0.24	0.07	0.04	0.02	0.213	0.5	0.425	1.0	0.213	0.35	0.427	1.2	0.07	0.05
W 51d-a[c]	0.153	11.5	0.068	12.8	0.080	9.64	0.092	3.12	0.063	4.11	0.063	2.96	3.86	3.26	3.41	0.130	70.2	0.183	77.6	0.107	10.6	0.203	16.5	6.62	4.70
(0,0)	0.107	0.15	0.107	0.07	0.285	0.14	0.104	0.09	0.104	0.06	0.278	0.11	0.13	0.05	0.14	0.213	0.19	0.425	0.38	0.213	0.16	0.427	0.42	0.10	0.12
W 51d-b[d]	0.153	21.0	0.068	34.0	0.080	45.2	0.092	6.18	0.063	9.86	0.063	16.5	3.56	3.61	2.87	0.130	153.6	0.183	221.7	0.107	21.7	0.203	56.4	7.08	3.93
(0,0)	0.107	0.22	0.107	0.11	0.285	0.19	0.104	0.13	0.104	0.09	0.278	0.15	0.08	0.03	0.03	0.213	0.3	0.425	0.5	0.213	0.2	0.427	0.6	0.07	0.04
DR 21	0.099	3.27	0.083	9.45			0.049	1.05	0.039	2.33			3.26	4.25		0.087	46.8	0.197	84.6	0.060	4.24	0.121	11.9	11.0	7.11
(0,0)	0.107	0.15	0.107	0.13			0.104	0.07	0.104	0.07			0.26	0.14		0.213	0.18	0.425	0.57	0.213	0.12	0.427	0.35	0.3	0.21
DR 21cal	0.112	12.0	0.120	25.2	0.098	40.2	0.045	3.51	0.045	7.86	0.054	15.0	3.57	3.36	2.81	0.150	97.2	0.234	153.1	0.116	14.9	0.280	40.6	6.52	3.77
(0,0)	0.107	0.17	0.107	0.18	0.285	0.25	0.104	0.07	0.104	0.07	0.278	0.13	0.08	0.04	0.03	0.213	0.35	0.425	0.72	0.213	0.27	0.427	0.93	0.12	0.09
DR 21OH	0.106	14.1	0.101	24.2	0.102	30.5	0.040	3.12	0.038	7.91	0.051	10.0	4.73	3.20	3.19	0.141	80.9	0.253	116.7	0.114	14.3	0.281	27.5	5.66	4.24
(0,0)	0.107	0.17	0.107	0.15	0.285	0.26	0.104	0.06	0.104	0.06	0.278	0.14	0.10	0.03	0.05	0.213	0.29	0.425	0.74	0.213	0.24	0.427	0.82	0.10	0.13
NGC 7538	0.040	8.09	0.050	18.7	0.042	37.4	0.030	2.88	0.030	4.79	0.082	11.3	2.94	3.91	4.09	0.119	103.2	0.146	167.1	0.086	11.3	0.191	29.3	9.13	5.70
(0,0)	0.107	0.07	0.107	0.08	0.285	0.11	0.104	0.05	0.104	0.05	0.278	0.22	0.06	0.04	0.05	0.213	0.3	0.425	0.6	0.213	0.25	0.427	0.79	0.20	0.16

[a]: Each source is characterized by two lines. First line, Col. 1: source name. Cols. 2 to 13: rms noise levels and integrated intensities (both in T_A^*) for the three ground rotational transitions intensities (of C^{18}O and of C^{17}O). Cols. 14 to 16: derived I(C^{18}O)/I(C^{17}O) integrated intensity ratios for the J=1–0, 2–1, and 3–2 transitions. Following Penzias (1981), the ratios were corrected for the difference in frequency of both isotopologues (increasing the ratios by a factor 1.047). Second line: Offset position, velocity resolution used and the uncertainties in the integrated intensities and line ratios.
Cols. 17 to 26: the same information as the Cols. 2 to 16, but for the simultaneously observed ^{13}CO and C^{18}O (1–0) and (2–1) transitions (the spectra of *these* C^{18}O observations are not shown in Fig. A.1.
[b] For L 134N and W 33 (0,0) using May 2000 C^{18}O(1–0) and August 1995 C^{17}O(1–O) spectra; [c]: for the 45–55 km s^{-1} component of W 51d; [d]: for the 55–75 km s^{-1} component of W 51d

be caused by differences in excitation and line opacities. Partial saturation of the stronger C^{18}O lines would lead to underestimated C^{18}O/C^{17}O abundance ratios. Since LVG calculations indicate $\tau_{(2-1)} > \tau_{(1-0)}$ for a wide range of parameters, saturation should be more pronounced in the 2–1 transitions, which may explain some of the very low ratios obtained with the 2–1 lines for sources of the inner Galaxy. Clouds heated by young massive stars (this holds for the overwhelming majority of our sources, see Table 2) should be warm enough to yield $\tau_{3-2} > \tau_{2-1}$ (the J=3 state is located ∼30 K above the J=0 level) which readily explains the relatively small J=3–2 C^{18}O/C^{17}O ratios, which are plotted in Fig. 1c.

Gradients may also be present in the ^{13}CO/C^{18}O J=1–0 and 2–1 ratios (Figs. 3a and b). If real, this can be explained by a lack

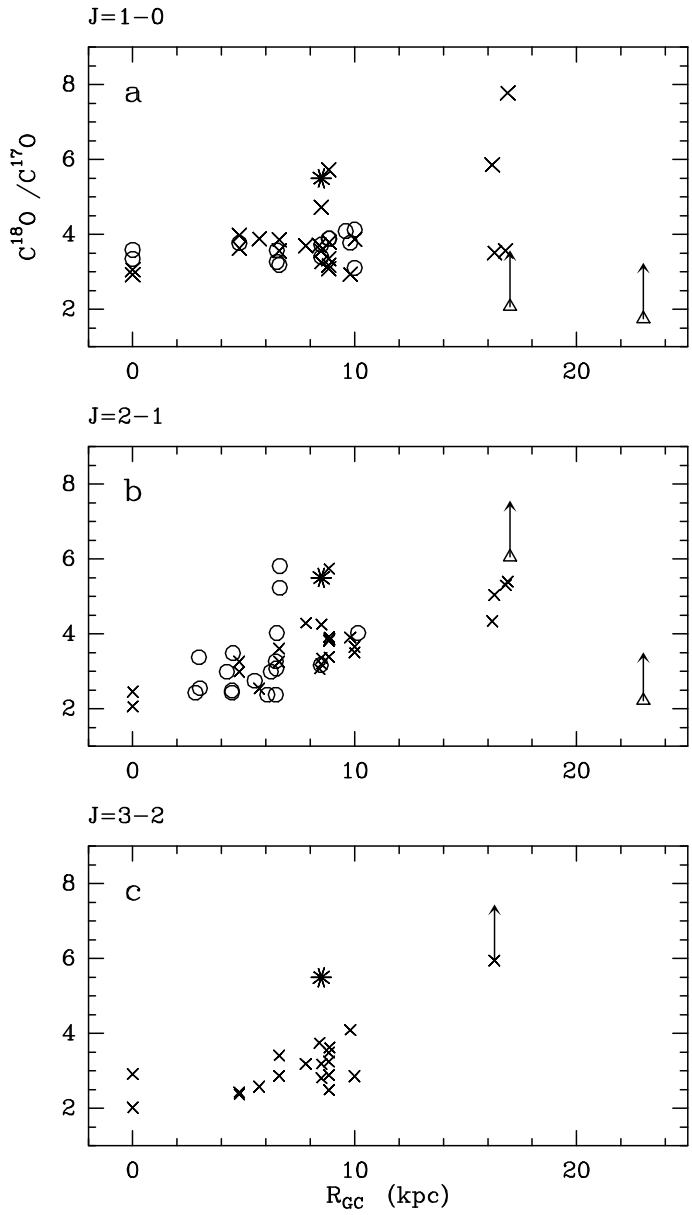


Fig. 1. $C^{18}O/C^{17}O$ abundance ratios, corrected for the difference between the $C^{18}O$ and $C^{17}O$ frequencies but not accounting for optical depth effects, in the **a)** J = 1–0, **b)** 2–1, and **c)** 3–2 transition as a function of distance from the galactic centre (R_{GC}). Crosses show our new results. Open triangles indicate 3σ lower limits for DDT94 Cloud 1 and 2 that motivated this study. Open circles represent J=1–0 line results from Penzias (1981) in **a)** and J=2–1 line results from Hofner et al. (2000) in **b)**. Error bars (see Table 3) have been omitted to avoid confusion. The solar system value of 5.5 is marked by an asterisk.

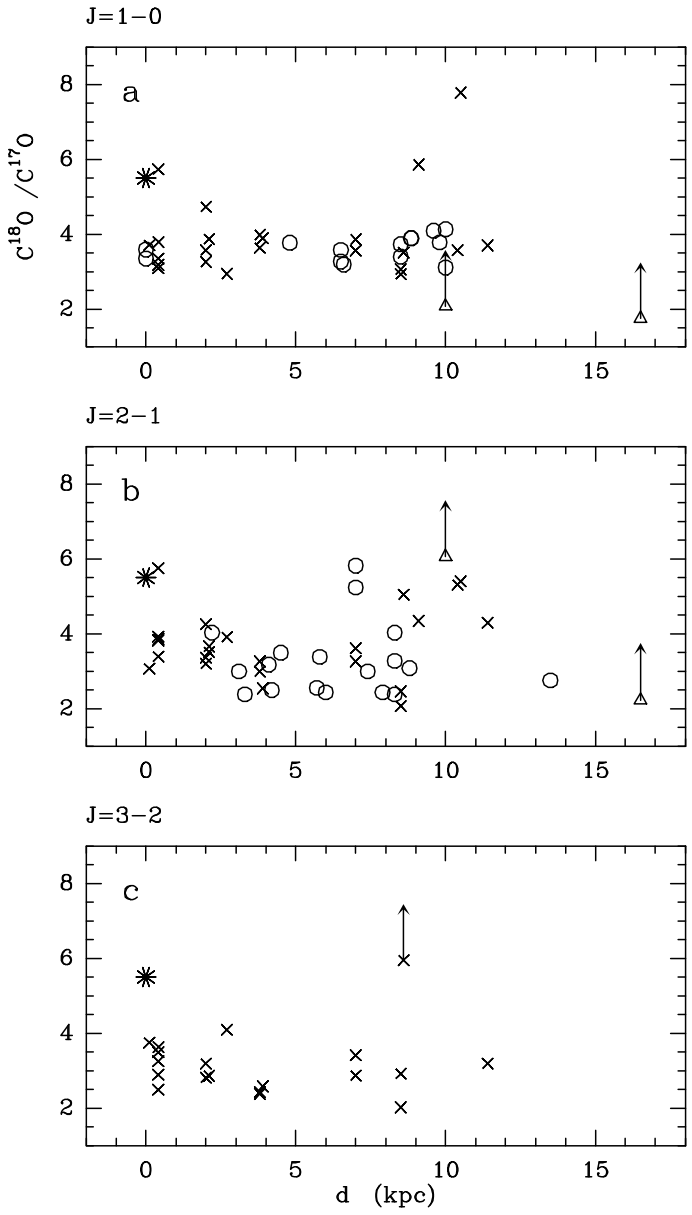


Fig. 2. The same as Fig. 1, but with distance from the Sun plotted instead of R_{GC}.

of diffuse gas in the high pressure environment of the galactic centre region, while sources further out may show large amounts of fractionated diffuse gas with enhanced ^{13}CO abundances (e.g., Watson et al. 1976; Bally & Langer 1982).

To directly determine optical depths, we fitted the relative strengths of the two $C^{17}O$ (1–0) groups of hyperfine components for sources with sufficiently small linewidths. In most cases, i.e. for WB89 391, WB89 437, WB89 501, Ori-KL (30,–240), and L134N, the optical depth of the $C^{17}O$(1–0) line is $\lesssim$0.1. Higher values for the $C^{17}O$ (1–0) optical depth were found towards WB89 380 (0.78±0.72), NGC 2024 (0.82±0.38; this source shows more than one velocity component, but a two-component fit did not provide a reliable value), Ori-KL (30,30) (0.76±0.34), and Ori-KL(0,−150) (0.27±0.53). In all of these cases, uncertainties are high. A one velocity component fit to the $C^{17}O$(2–1) transition could only be obtained towards L134N: τ=0.53±0.11. Assuming $\tau[C^{18}O(1–0)] \sim 4\times\tau[C^{17}O(1–0)]$, these results suggest that $\tau(C^{18}O(1–0))$ is commonly *but not always* smaller than unity and that $\tau[C^{18}O(2–1)] > \tau[C^{18}O(1–0)]$. Figs. 3c supports this finding, indicating no saturation effects in the J=1–0 lines. $C^{18}O/C^{17}O$ appears to be independent of $^{13}CO/C^{18}O$. The opposite appears, however, to hold for the 2–1 lines. Here small $^{13}CO/C^{18}O$ ratios are accompanied by small $C^{18}O/C^{17}O$ values, suggesting some degree of ^{13}CO and $C^{18}O$ J=2–1 line saturation.

Towards all sources we observed one or a few positions only. A map of the Orion-KL cloud was, however, made by White & Sandell (1995) in the $C^{18}O$ and $C^{17}O$ (2–1) transitions. Although

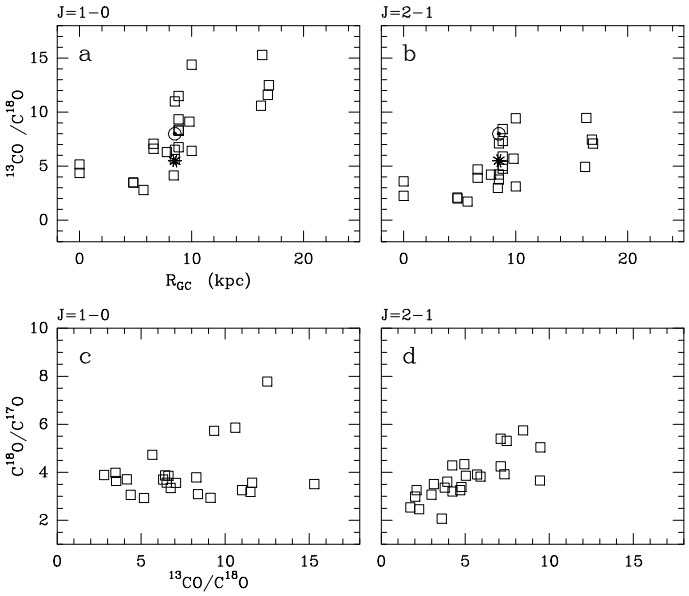


Fig. 3. $^{13}CO/C^{18}O$ integrated intensity ratios in the **a)** J = 1–0 and **b)** 2–1 transition as a function of distance from the galactic centre (R_{GC}). Open squares indicate our new results. The values for the solar system of 5.5 (circle with central dot) and for the solar neighbourhood of 8.0 (asterisk) are also indicated. **c)** The $C^{18}O/C^{17}O$ integrated intensity ratio as a function of $^{13}CO/C^{18}O$ for the J=1–0 and **d)** J=2–1 transition.

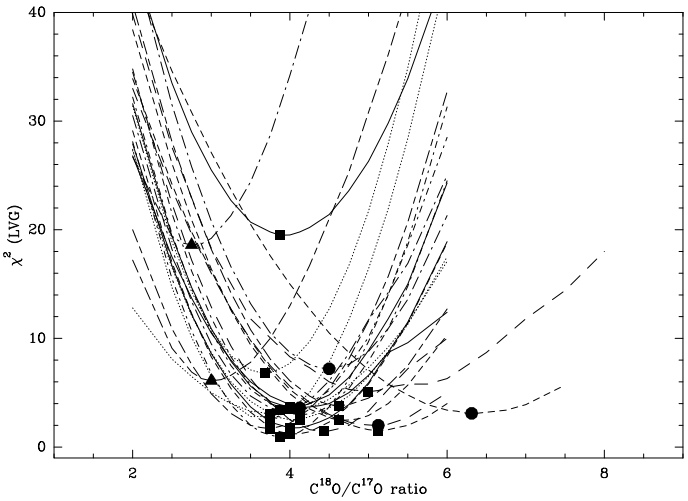


Fig. 4. Results of LVG simulations modeling our sample of sources: χ^2 as a function of assumed $C^{18}O/C^{17}O$ ratio. The minimum χ^2 values are indicated by filled triangles (Sgr B2), squares (3kpc<R_{GC}<10kpc), and circles (R_{GC}>16kpc). The calculations were made with steps of 0.125 (near the minimum χ^2) to 0.50 in the $C^{18}O/C^{17}O$ ratio. The $C^{18}O/H_2$ abundance ratio was assumed to be 1.7 10^{-7} (Frerking et al. 1982). The results are similar to those also accounting for a galactic $C^{18}O/H_2$ abundance gradient.

their primary goal was not the determination of $^{18}O/^{17}O$ abundance ratios, their Fig. 8 might indicate a surprising trend towards larger $C^{18}O/C^{17}O$ ratios at larger extinctions or $C^{18}O$ column densities that deserves further study. Our value for Ori-KL (0,0) (both for the J=1–0 and 2–1 lines) is consistent with the ratios found by White & Sandell (1995) at high A_v.

4.2. LVG calculations

4.2.1. Models with $C^{18}O/H_2 = 1.7\times10^{-7}$

For all sources the combined data sets (excluding ^{13}CO, because some of it probably originates from a more diffuse lower density environment) have been analysed with an LVG code, in the same way as done by Wouterloot et al. (2005) for the ρ Oph cloud. We used rates by Flower (2001) for collisions with H_2 and assumed an ortho/para H_2 abundance ratio of three (our results are not sensitively dependent on this value). For L134N, a cold dark cloud, the same parameter space was used as for ρ Oph in Wouterloot et al. (2005) (5 K $\leq T_{kin} \leq$ 35 K, 10^3 cm^{-3} $\leq n(H_2) \leq 10^6$ cm^{-3}, and $2.0 \leq C^{18}O/C^{17}O \leq 6.0$). For the other sources T_{kin} ranged from 5 K to 100 K or even 130 K (for DR21cal) using the same range of densities and $C^{18}O/C^{17}O$ ratios as for L134N. In all cases the adopted velocity gradient was 5.0 kms^{-1}pc^{-1} that roughly reflects cloud size and measured linewidths.

The models were compared with the observations by calculating χ^2 values from the $C^{18}O$ peak temperatures and the $C^{18}O/C^{17}O$ ratios, using for the latter integrated line temperatures. For this procedure, the observed peak T_A^* temperatures of $C^{18}O$ were converted to T_{mb} temperatures except for L134N, where the emission is much less peaked at the observed position than for the other sources (see e.g., Pratap et al. 2000). The J=2–1 and 3–2 peak temperatures used are those of spectra that were convolved to the J=1–0 resolution using results from the $C^{18}O$ (2–1) HERA maps. For the uncertainties we assumed a calibration error of ±10% in the line temperatures and of ±14% in the line ratios (see Sect. 2.3). In Fig. 4, χ^2 is shown as a function of the adopted $C^{18}O/C^{17}O$ ratio. This ratio was varied in steps of 0.125 (near the minimum χ^2) to 0.5. For these models we assumed the Frerking et al. (1982) $C^{18}O/H_2$ abundance ratio of 1.7 10^{-7}. All sources show a well-defined minimum. The parameters of the model with the lowest χ^2 are listed in Table 4, Col. 4.

The average $C^{18}O/C^{17}O$ ratio is 4.18±0.15. Excluding the two positions towards Sgr B2, which have low ratios (2.88±0.11), and the objects at R_{GC}>16kpc, which have high values (5.02±0.45), the average ratio becomes 4.15±0.10. This is close to the values (4.11±0.14 and 4.13±0.13) derived for ρ Oph and NGC 6334 FIR II by Wouterloot et al. (2005) and Zhang et al. (2007), respectively.

4.2.2. Introducing a $C^{18}O$ abundance gradient

From optical and FIR observations it has been shown that many metals show a considerable abundance gradient. Abundances decrease from the galactic centre to larger R_{GC} (e.g., Rudolph et al. 2006). Gradients amount to −0.078 dex/kpc for $^{14}N/H$, −0.051 dex/kpc for $^{16}O/H$, and −0.044 dex/kpc for $^{32}S/H$ (these are average values from optical and FIR measurements which yield slightly different results). For $^{12}C/H$, there are only few data. Rolleston et al. (2000) obtained a slope of −0.070 dex/kpc from 80 stars in 19 open clusters (6≤R_{GC}≤18kpc). Esteban et al. (2005) observed recombination lines towards 8 HII regions (6.3 ≤ R_{GC} ≤ 10.4kpc) and derived a slope of −0.103 dex/kpc. Model calculations by Matteucci & François (1989) suggest a gradient of −0.066 dex/kpc for $^{12}C/H$. In all cases, where measurements extend to large galactocentric radii, there is no sign for a change in the radial gradient.

In addition to the gradients in the ^{12}C and ^{16}O abundances, there is also a gradient in the $^{16}O/^{18}O$ ratio: Wilson & Rood (1994) give a ratio of ∼250 for the galactic centre region and

Table 4. Results of LVG model calculations[a].

Nr	Source	Offset (arcsec)	$C^{18}O/C^{17}O$	T_{kin} (K)	log $n(H_2)$ (cm^{-3})	χ^2	$C^{18}O/C^{17}O$	T_{kin} (K)	log $n(H_2)$ cm^{-3}	χ^2	R_{GC} kpc
			$C^{18}O/H_2$ Frerking				$C^{18}O/H_2$ Frerking+gradient				
1	WB89 380	0,0	4.13	77.5	4.0	3.6	4.13	45.0	4.8	3.4	16.8
2	WB89 391	0,0	6.31	70.0	4.1	3.1	6.38	45.0	4.9	2.6	16.9
3	W 3	0,0	3.75	25.0	4.3	3.0	3.88	25.0	4.5	6.2	10.0
4	W 3OH	0,0	3.88	30.0	4.8	0.9	3.88	27.5	4.9	1.6	10.0
5	WB89 437	0,0	5.13	30.0	4.0	2.0	5.13	20.0	4.7	2.4	16.2
6	WB89 501	0,0	4.5	60.0	3.9	7.2	4.5	20.0	4.7	16.4	16.3
7	Ori KL	0,0	3.88	52.5	4.9	19.5	3.88	62.5	5.0	19.1	8.84
8	Ori KL	30,30	4.0	45.0	5.3	1.2	4.13	42.5	5.3	2.1	8.84
9	Ori KL	0,–150	3.75	45.0	4.9	2.4	3.75	52.5	5.0	2.4	8.84
10	Ori KL	30,–240	4.0	40.0	5.0	3.5	4.0	37.5	5.0	4.8	8.84
11	NGC 2024	0,0	4.63	20.0	4.8	3.8	4.5	20.0	4.8	5.7	8.86
12	L 134N	0,0	5.0	7.0	4.7	5.1	5.0	7.0	4.6	5.6	8.41
13	Sgr B2M	0,0	3.0	37.5	5.1	6.1	3.0	42.5	4.3	5.3	0.1
14	Sgr B2M	0,15	2.75	35.0	4.8	18.6	2.75	57.5	3.9	21.5	0.1
15	W33	0,0	4.0	30.0	5.1	1.8	4.25	30.0	4.8	1.1	4.8
16	W33	0,24	5.13	30.0	5.5	1.5	4.75	32.5	5.0	1.6	4.8
17	G34.3+0.2	0,0	4.13	35.0	5.3	2.5	4.13	35.0	5.0	2.2	5.7
18	W49N	0,0	4.13	50.0	5.0	3.0	4.25	45.0	4.9	3.2	7.8
19	W51d-a[b]	0,0	4.44	12.5	4.7	1.5	4.5	12.5	4.4	1.3	6.6
20	W51d-b[b]	0,0	3.88	25.0	4.8	3.4	4.0	25.0	4.7	3.6	6.6
21	DR 21	0,0	3.75	107.5	4.7	1.7	3.75	107.5	4.7	1.7	8.5
22	DR 21cal	0,0	4.0	30.0	5.0	3.7	4.0	30.0	5.0	3.7	8.5
23	DR 21OH	0,0	4.63	22.5	4.9	2.5	4.63	22.5	4.9	2.5	8.5
24	NGC 7538	0,0	3.69	40.0	4.8	6.8	3.63	40.0	4.9	6.7	9.8

[a]: Cols. 2 and 3: source and offset; Cols. 4 to 7: derived $C^{18}O/C^{17}O$ ratio, kinetic temperature, H_2 density and minimum χ^2.
Cols. 8 to 11: the same parameters as Cols. 4 to 7, but for the case of a galactic $C^{18}O/H_2$ abundance gradient (see Sects. 4.1 and 4.2).
[b]: W51d-a: 50 km s^{-1} component; W51d-b: 60 km s^{-1} component (see Fig. A.1).

a fitted ratio of $^{16}O/^{18}O \sim (59\pm12)\times R_{GC} + (37\pm83)$ for larger R_{GC} values ($2.8 \le R_{GC} \le 9$ kpc).

Adopting the above mentioned $^{16}O/H$ abundance gradient of −0.051 dex/kpc, the oxygen abundance becomes a factor of 2.7 higher near the galactic centre and a factor of 2.4 lower at R_{GC} = 16 kpc than in the solar neighbourhood. Similarly, the $^{16}O/^{18}O$ ratio is then factor of 2.1 lower near the centre (using a minimum $^{16}O/^{18}O$ ratio of 250) and a factor of 1.8 higher at R_{GC} = 16 kpc than the fitted value near the Sun, 537 (Wilson & Rood 1994) which can be compared with the solar system value of 490 (Anders & Grevesse 1989).

Applying both gradients to estimate $^{18}O/H$, the ratios become a factor of 5.7 higher at the centre and a factor of 4.4 lower at R_{GC} = 16 kpc than in the solar neighbourhood. Taking for ^{12}C the mean of the gradients determined by Rolleston et al. (2000) and Esteban et al. (2005), –0.0865 dex/kpc, we obtain $^{12}C/H$ abundances that vary between 5.4 higher and 4.5 times lower within the same range of galactocentric radii. Since the gradients are uncertain and the true abundances also depend on chemical reactions in the clouds, the $^{18}O/H$ and $^{12}C/H$ gradients are identical within the error limits. In our LVG calculations we have therefore used the $^{18}O/H$ gradient for all sources to obtain a second estimate of $^{18}O/^{17}O$ ratios. For large R_{GC}, the extrapolated lower abundances are consistent with chemical model calculations (Ruffle et al. 2007) simulating multi-line measurements of DDT94 Cloud 2.

The results are given in Table 4 (Cols. 7 to 10) and Fig. 5. There is little change in the $C^{18}O/C^{17}O$ ratios compared to those without considering the abundance gradient (Col. 4 of Table 4). The average $C^{18}O/C^{17}O$ ratio becomes 4.20±0.14 instead of 4.18±0.15. Excluding the two positions in Sgr B2, which have low ratios (2.88±0.11), and the objects at R_{GC}>16kpc, which have higher values (5.03±0.46), the average ratio becomes 4.16±0.09. This is again close to the value derived by Wouterloot et al. (2005) for ρ Oph (see also Zhang et al. 2007 for NGC6334 FIR II). There are, however, differences in the derived kinetic temperatures and densities. In the first set of models (with fixed $C^{18}O/H_2$ abundance ratios) the derived densities are significantly smaller at R_{GC}>16kpc than for 3<R_{GC}<10kpc. This difference is greatly reduced in the second set of models accounting for $C^{18}O/H_2$ gradients (Fig. 6). If we assume that the H_2 densities in star forming clumps such as those in our selected sample are similar at all locations in the Galaxy, this indicates that the models with the abundance gradient are more realistic.

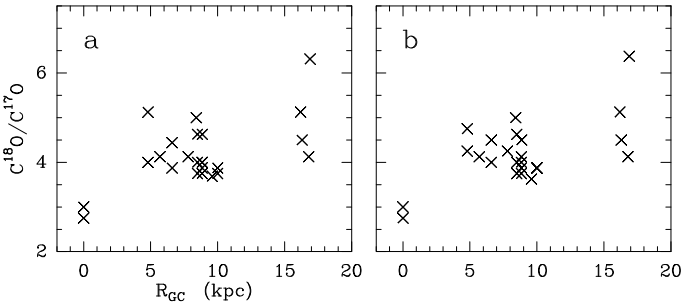


Fig. 5. Results of LVG calculations: The $C^{18}O/C^{17}O$ ratio as a function of R_{GC}. **a)** The $C^{18}O/H_2$ ratio was assumed to be 1.7 10^{-7} (Frerking et al. 1982), or **b)** corrected for the galactic abundance gradients (see Sect. 4.2.2).

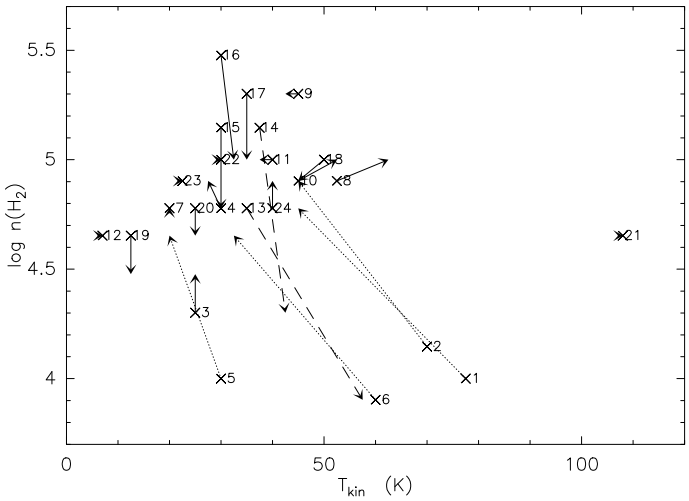


Fig. 6. Results of LVG calculations: The crosses indicate the best fit $T_{\rm kin}$ and $n(H_2)$ using the Frerking et al. (1982) abundance. The arrows point to the results for the model using an abundance gradient. The arrows for the clouds at R>16kpc are dotted, those for Sgr B2 are dashed. Numbers indicate the sequential line-of-sight number, indicated in Table 4.

4.2.3. Implications

The two sets of models, either ignoring or accounting for radial $C^{18}O/H_2$ abundance gradients across the Galaxy, suggest the existence of a $C^{18}O/C^{17}O$ gradient from values slightly smaller than three near the galactic centre to values around five at large galactocentric radii (Fig. 5). The $^{18}O/^{17}O$ ratio of Sgr B2 deduced from HCO^+, 3.1±0.6 (Guélin et al. 1982), is consistent with this result. Our results do suggest that the $C^{18}O/C^{17}O$ ratio at 4 to 11 kpc from the galactic centre is larger than the value derived by Penzias (1981; 3.65±0.15). The reason is that the J=1–0 results from Penzias were not corrected for radiative transfer effects.

^{18}O is synthesised by helium burning on ^{14}N in massive stars. ^{14}N is a mostly secondary nucleus so that its abundance is highly metallicity-dependent, with low N/C and N/O abundance ratios at low metallicities (e.g., Wheeler et al. 1989). ^{18}O may follow this trend. ^{17}O is mainly a product of CNO-hydrogen burning and is also released by stars of intermediate mass (for yields, see, e.g., Prantzos et al. 1996).

To qualitatively reproduce the $^{18}O/^{17}O$ ratios observed in interstellar clouds and stellar objects, we should note that in individual dust grains from massive stars ^{18}O overabundances of up to two orders of magnitude can be reached (e.g., Amari et al. 1995). Low ratios, sometimes below unity, are obtained towards late-type stars of intermediate mass (c.f., Sect. 1). The low values indicate that ^{18}O is destroyed in such stars (see also Henkel & Mauersberger 1993; Henkel et al. 1994).

For the Large Magellanic Cloud (LMC), the $C^{18}O/C^{17}O$ (2–1) ratio has been studied by Heikkilä et al. (1998). These Clouds have even lower metallicities than the far outer Galaxy and are characterised by $C^{18}O/C^{17}O \sim 1.6$, which is significantly lower than all measured interstellar values in the Galaxy. The LMC, which undergoes a phase of enhanced massive star formation, is metal-poor so that its ^{18}O abundance should be low. Very high $C^{18}O/C^{17}O$ ratios are instead found in nuclear starbursts (e.g., Harrison et al. 1999; Wang et al. 2004). This may be a consequence of (1) high metallicities and (2) large amounts of ejecta from massive stars that must have enriched the interstellar medium.

In the central region of our Galaxy, metallicities are also high. However, here CNO burning dominates resulting isotope ratios of C, N, and O. Apparently, a nuclear starburst with large numbers of massive stars has not contaminated the galactic centre region since a long time. Products from helium burning are therefore underepresented in the C, N, and O isotope abundances, yielding a very low $^{12}C/^{13}C$ ratio (∼25), an extremely large $^{14}N/^{15}N$ ratio (of order 1000) (e.g., Wilson & Rood 1994) and the low $^{18}O/^{17}O$ ratio ($\lesssim 3$) proposed here.

What remains, at first sight, puzzling is (1) that there exists a galactic disc $^{18}O/^{17}O$ gradient and (2) that the high $^{18}O/^{17}O$ ratios in the metal-poor outer Galaxy do not match the low values in the even more metal-poor LMC. Does this latter discrepancy imply that the metallicities of the outer Galaxy still permit efficient high-mass star production of ^{18}O? While the LMC is too metal-poor to make the process efficient? Or that, in spite of the presently visible large numbers of massive stars the LMC starburst is still too young to enrich the interstellar medium with ^{18}O-rich ejecta? Both possibilities appear to be farfetched. The first, because the metallicities are not that different (e.g., Hunter et al. 2007; Ruffle et al. 2007) to justify an extreme variation (by a factor of three) between measured $^{18}O/^{17}O$ ratios, the second, because the starburst in the LMC started as early as 50×10^6 yr ago (e.g., Westerlund 1990).

The galactic gradient and the difference between outer Galaxy and LMC may instead be interpreted in terms of current models of galacto-chemical evolution. The most accepted mechanism to explain the existence of abundance gradients is the so-called "biased infall" (e.g., Chiappini & Mateucci 1999) with the galactic disc being slowly formed from inside out. In such a scenario, ^{18}O abundances may be low in both the outer disc and LMC and the difference is mainly caused by ^{17}O. In the LMC, where star formation is ongoing since at least 10^{10} yr (e.g., Hodge 1989), there was sufficient time to form ^{17}O predominantly from stars of intermediate mass. The outer Galaxy, however, may be too young to build up a similar ^{17}O abundance, with timescales (and abundances) rapidly decreasing the farther out the measured molecular cloud is located.

To summarise, we *may have found a fundamental difference between the metal-poor outer regions of the Galaxy and the metal-poor LMC.* Generalizing this result, the difference implies that the abundances of the outer regions of spirals cannot be considered to be intermediate between those found near the solar circle and those determined in small metal-poor dwarf galaxies. As a cautionary note, however, we have to emphasise that *the $^{18}O/^{17}O$ ratios of the innermost and outermost galactic star-forming regions are still based on a very small number of targets.* Additional data to confirm or to reject the trend of rising $^{18}O/^{17}O$ ratios with galactocentric radius would thus be highly desirable.

5. Conclusions

To measure interstellar $^{18}O/^{17}O$ ratios, we observed three $C^{18}O$ and $C^{17}O$ transitions towards 25 positions in 18 galactic sources located at galactocentric distances $0\,{\rm kpc} \le R_{\rm GC} \le 16.9\,{\rm kpc}$. These measurements are complemented by ^{13}CO observations in the two ground rotational transitions. $C^{18}O/C^{17}O$ line intensity ratios from the J=2–1 and 3–2 transitions are lower than those from the 1–0 lines, indicating that optical depth effects have to be considered. This is also suggested by a comparison with the ^{13}CO (1–0) and (2–1) spectra.

Therefore, all $C^{18}O$ and $C^{17}O$ observations were combined by means of LVG calculations. This was done assuming (1) that the $C^{18}O/H_2$ abundance ratio is constant throughout the Galaxy and (2) that there is a radial $C^{18}O/H_2$ abundance gradient. These assumptions do not affect significantly the final $C^{18}O/C^{17}O$ values, which should provide a good approximation to the $^{18}O/^{17}O$ isotope ratio. For the central region, $^{18}O/^{17}O = 2.88\pm0.11$. For R_{GC} = 4–11 kpc, the ratio becomes 4.16±0.09. In the outer Galaxy (16 kpc $\leq R_{GC} \leq$ 17 kpc), we find 5.03±0.46.

The low ratio in the galactic centre region is consistent with a CNO-hydrogen burning dominated nucleosynthesis that is also characterizing the carbon and nitrogen isotope ratios. It supports the view that ^{18}O is predominantly synthesised in high-mass stars, while ^{17}O is predominantly a product of stars of lower mass. The ratio between 4 and 11 kpc is consistent with recent results from a few "local" individual clouds. It is smaller than the solar system ratio (5.5), suggesting that the Sun was enriched by material from massive stars during its formation. The $^{18}O/^{17}O$ values measured for the outer Galaxy are more difficult to interpret. They are not low, as in the case of the metal-poor massive star forming Large Magellanic Cloud but appear to be higher than anywhere else in the interstellar medium of the Galaxy. This and the galactic disc gradient may be explained by the small age of the outer galactic disc and may imply that the metal-poor outer reaches of spiral galaxies provide quite different environments than similarly metal-poor dwarf galaxies. Nevertheless, both the Galactic centre and outer Galaxy $^{18}O/^{17}O$ isotope ratios suffer from small number statistics so that more observations are needed to confirm or to reject the trend found in this study.

References

Anders E., & Grevesse N. 1989, Geochim. Cosmochim. Acta 53, 197
Amari, S., Zinner, E., & Lewis, R. S. 1995, ApJ, 447, L147
Anthony-Twarog, B,J., 1982, AJ 87, 1213
Bally, J., & Langer, W. D. 1982, ApJ, 255, 143
Bensch, F., Pak, I., Wouterloot, J. G. A., Klapper, G., & Winnewisser, G. 2001, ApJ, 591, 1013
Bieging, J. 1997, Radio observations of the isotopic composition of the Galaxy. In: T.J. Bernatowicz, E. Zinner (eds.) The Astrophysical Implications of the Laboratory Study of Presolar Materials, AIP Conf. Proc., 402, p. 407
Brand, J., & Blitz, L. 1993, A&A, 275, 67
Brand, J., & Wouterloot, J.G.A. 1994, A&AS 103, 503
Brand, J., & Wouterloot, J.G.A. 1995, A&A 303, 851
Chiappini, C., & Matteucci, F. 1999, ApS&S, 265, 425
Dickel, J. R., Dickel, H. R., & Wilson, W. J. 1978, ApJ, 223, 840
Digel, S., de Geus, E., & Thaddeus, P. 1994, ApJ, 422, 92 (DDT94)
Eisenhauer, F., Genzel, R., Alexander, T., et al. 2005, ApJ, 628, 246
Esteban, C., Garcia-Rojas, J., Peimbert, M., et al. 2005, ApJ, 618, 95
Flower, D. R. 2001, J. Phys. B: At. Mol. Opt. Phys., 34, 1
Franco, G. A. P. 1989, A&A, 223,313
Frerking, M. A., Langer, W. D., & Wilson, R. W. 1982, ApJ, 262, 590
Guélin, M., Cernicharo, J., & Linke R. A. 1982, ApJ, 263, L89
Gwinn, C.R., Moran, J.M., Reid, M.J. 1992, ApJ 393, 149
Hachisuka, K., Brunthaler, A., Menten, K.M., 2006, ApJ 645, 337
Harrison, A., Henkel, C., & Russell, A. 1999, MNRAS, 303, 157
Heger, A., & Langer, N. 2000, ApJ, 544, 1016
Heikkilä, R., Johanssson, L. E. B., & Olofsson H. 1998, A&A, 332, 493
Henkel, C., & Mauersberger, R. 1993, A&A, 274, 730
Henkel, C., Wilson, T.L., Langer, N., Chin, Y.-N., & Mauersberger, R. 1994, Interstellar CNO isotope ratios. In: Wilson T.L., Johnson K.J. (eds.) Structure and content of molecular clouds. Springer-Verlag, Berlin, p. 72
Hodge, P. 1989, ARA&A, 27, 139
Hoffman, R. D., Woosley, S. E, & Weaver, T. A. 2001, ApJ, 549, 1085
Hofner, P., Wyrowski, F., Walmsley, C. M., & Churchwell, E. 2000, ApJ, 536, 393
Hüttemeister, S., Dahmen, G., Mauersberger, R., et al. 1998, A&A, 334, 646
Hunter, I., Dufton, P. L., Smartt, S. J., et al. 2007, A&A, 466, 277
Ibata, R. A., Gilmore, G., & Irwin, M. J. 1995, MNRAS, 277, 781
Imai, H., Kameya, O,m Sasao, T., et al. 2000, ApJ 538, 751
Kahane, C. 1995, Isotopic abundances in the interstellar medium and circumstellar envelopes. In: M. Busso et al. (eds.) Nuclei in the Cosmos, AIP Conf. Proc., 327, p. 19
Kahane, C., Cernicharo, J., Gomez-Gonzalez, J., & Guelin, M. 1992, A&A, 256, 235
Kerr, F.J., & Lynden-Bell, D. 1986, MNRAS 221, 1023
Lacy J.H., Jaffe, D.T., Zhu, Q., et al. 2007, ApJ 658, L45
Langer, W. D., Graedel, T. E., Frerking M. A., & Armentrout, P. B. 1984, ApJ, 277, 581
Langer, N., & Henkel, C. 1995, Space Sci. Rev., 74, 343
Linke, R. A., Goldsmith, P. F., Wannier, P. G., Wilson, R. W., & Penzias, A. A. 1977, ApJ, 214, 581
Matteucci, F., & François 1989, MNRAS, 239, 885
Mauersberger, R., Guélin, M., Martin-Pintado J., et al. 1989, A&AS, 79, 217
Menten, K.M., Reid, M.J., Forbrich, J., Brunthaler, A. 2007, A&A 474, 515
Penzias, A. A. 1981, ApJ, 249, 518
Prantzos, N., Aubert, O., & Audouze, J. 1996, A&A, 309, 760
Pratap, P., Megeath, S. T., & Bergin, E. A. 2000, ApJ, 542, 870
Rohlfs, K., & Wilson, T.L. 1996, Tools of Radio Astronomy. Springer-Verlag, Berlin, p. 194
Rolleston, W. R. J., Smartt, S. J., Dufton, P. L., & Ryans, R.S.I. 2000, A&A, 367, 86
Rudolph, A. R., Fich, M., Bell, G. R., et al. 2006, ApJS, 162, 346
Ruffle, P. M. E., Millar, T. J., Roberts, H., et al. 2007, ApJ, 671, 1766
Smartt, S. J., Dufton, P. L., & Rolleston, W. R. J. 1996, A&A, 305, 164
Stoesz, J. A., & Herwig, F. 2003, MNRAS, 340, 763
Wang, M., Henkel, C., Chin, Y.-N., et al. 2004, A&A, 422, 883
Watson, W. D., Anicich, V. G., & Huntress, W. T. 1976, ApJ, 205, L165
Westerlund, B. E. 1990, A&AR, 2, 29
Wheeler, J. C., Sneden, C., & Truran, J. W. 1989, ARA&A, 27, 279
White, G. J., & Sandell, G. 1995, A&A, 299, 179
Wilking, B. G., & Lada, C. J. 1983, ApJ, 274, 698
Wilson, T. L., & Matteucci, F. 1992, A&AR, 4, 1
Wilson, T. L., & Rood, R. T. 1994, ARA&A, 32, 191
Wouterloot, J. G. A., & Brand, J. 1989, A&AS, 80, 149
Wouterloot, J. G. A., & Brand, J. 1996, A&AS, 119, 439
Wouterloot, J.G.A., Brand, J., & Henkel, C. 2005, A&A, 430, 549
Xu, Y., Reid, M.J., Zheng, X.W., Menten, K.M. 2006, Science 311, 54
Zhang, J., Henkel, C., Mauersberger, R., et al. 2007, A&A, 465, 887

Online Material

Appendix A: Spectra

List of Objects

‘DDT94 Cloud 1’ on page 2
‘DDT94 Cloud 2’ on page 2
‘WB89 380’ on page 4
‘WB89 391’ on page 4
‘DDT94 Cloud 1’ on page 4
‘W 3’ on page 4
‘W 3OH’ on page 4
‘WB89 437’ on page 4
‘DDT94 Cloud 2’ on page 4
‘WB89 501’ on page 4
‘Ori KL’ on page 4
‘NGC 2024’ on page 4
‘L 134N’ on page 4
‘Sgr B2(M)’ on page 4
‘W 33’ on page 4
‘G34.3+0.2’ on page 4
‘W 49N’ on page 4
‘W 51’ on page 4
‘DR 21’ on page 4
‘DR 21OH’ on page 4
‘NGC 7538’ on page 4

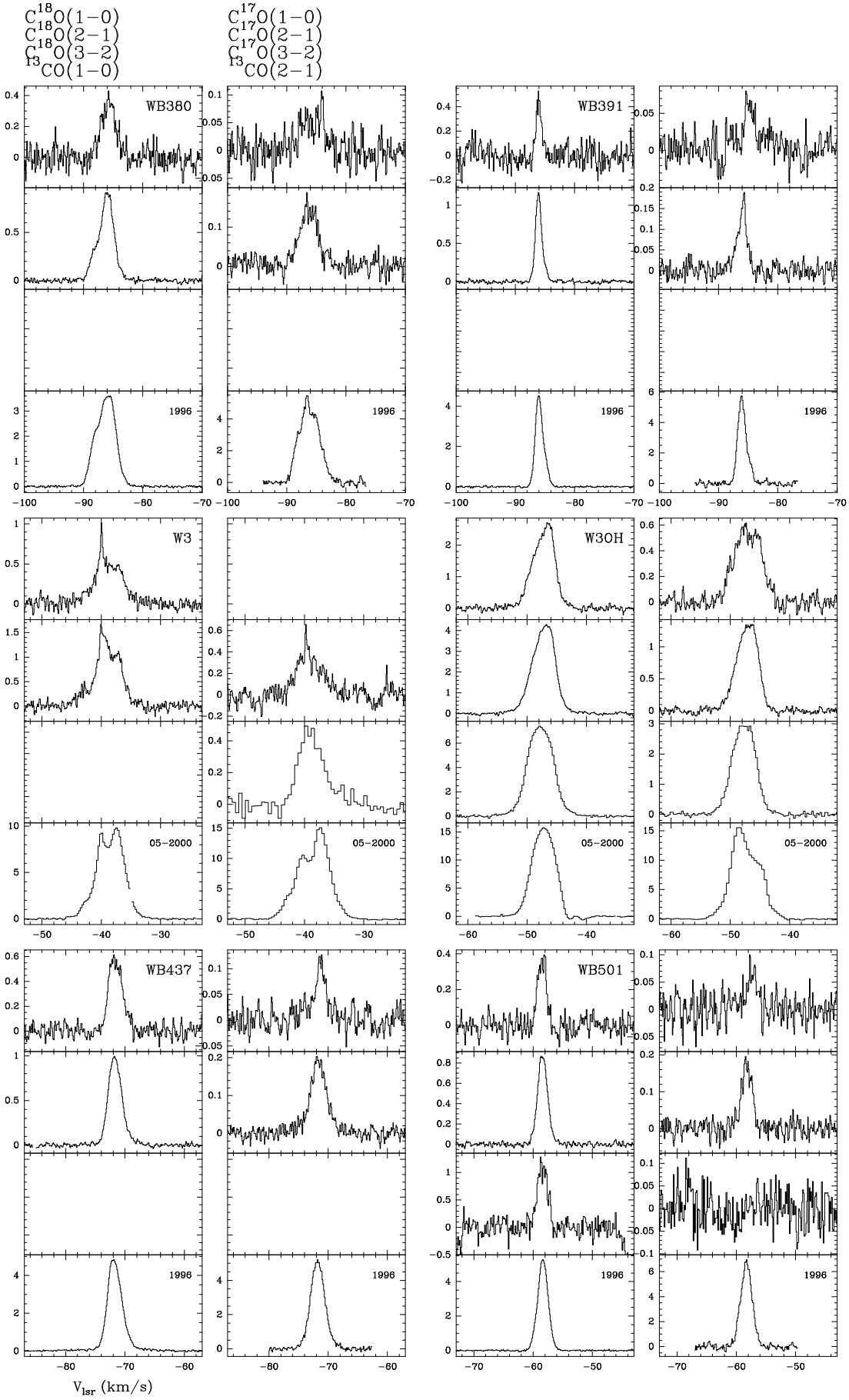


Fig. A.1. $C^{17}O$, $C^{18}O$ J = 1–0, 2–1, and 3–2, and ^{13}CO J = 1–0 and 2–1 spectra. In most cases the velocity range is 30 km s^{-1}, except for a few sources with very broad lines.

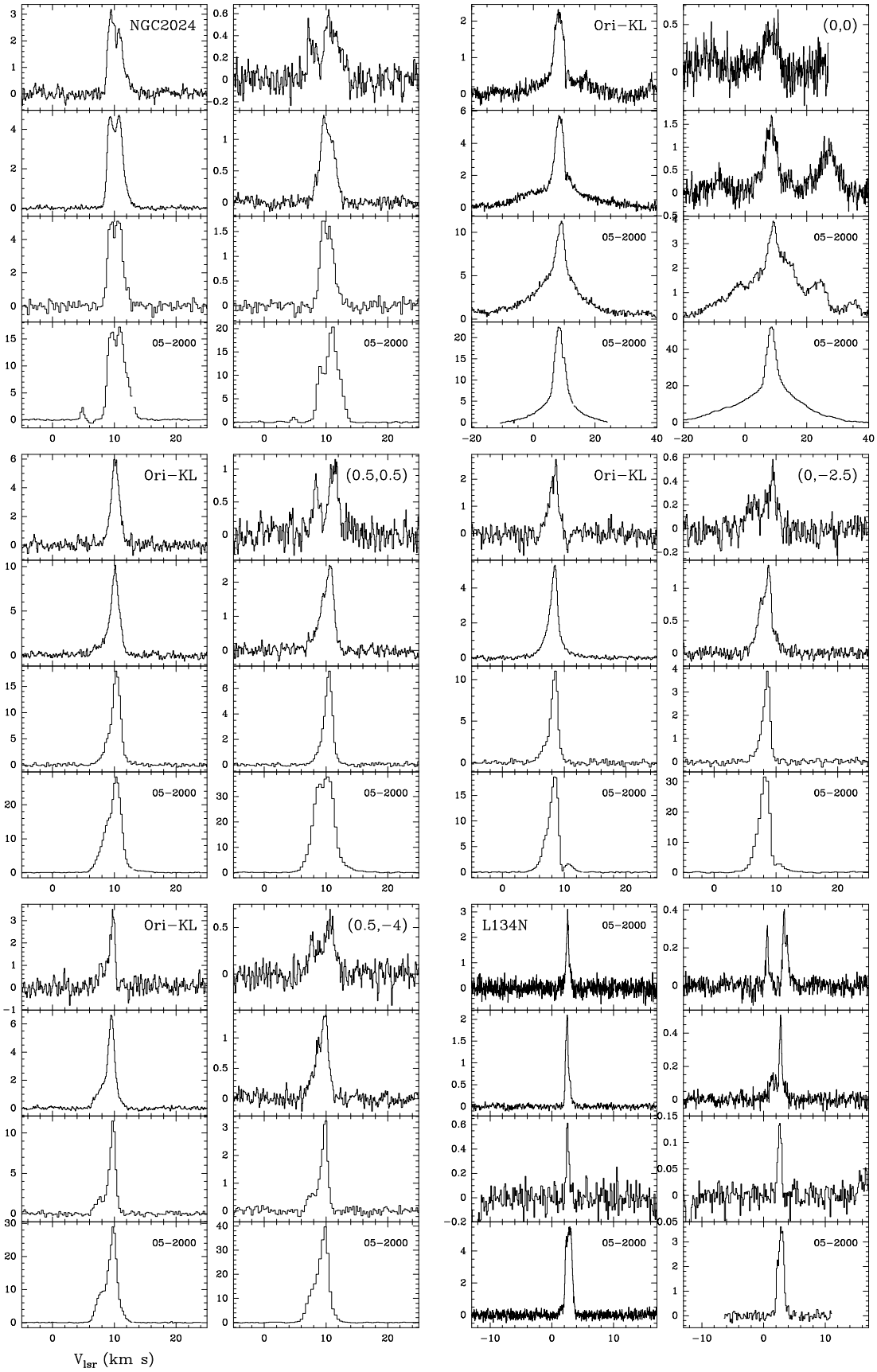


Fig. A.1. Continued.

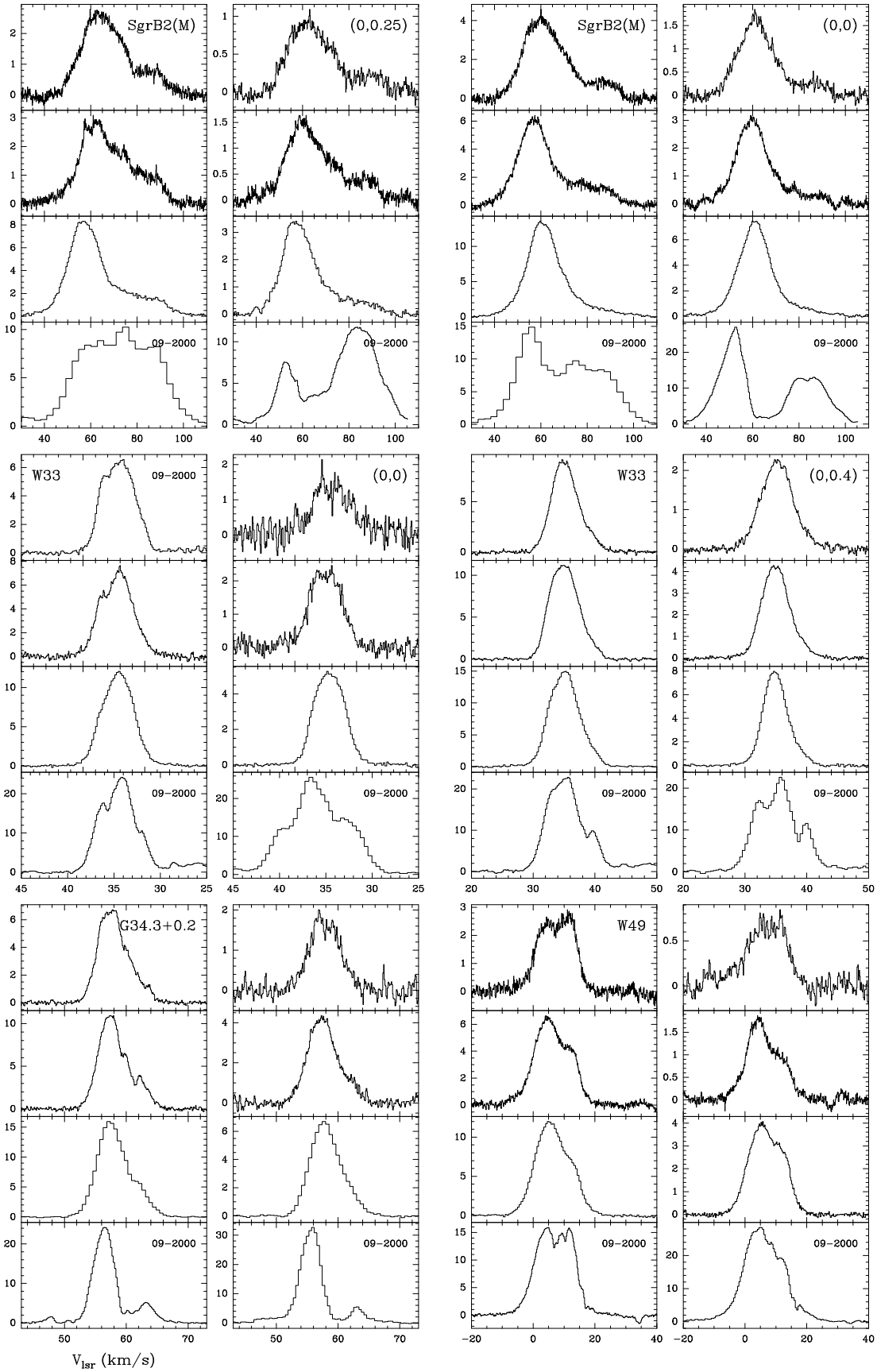


Fig. A.1. Continued.

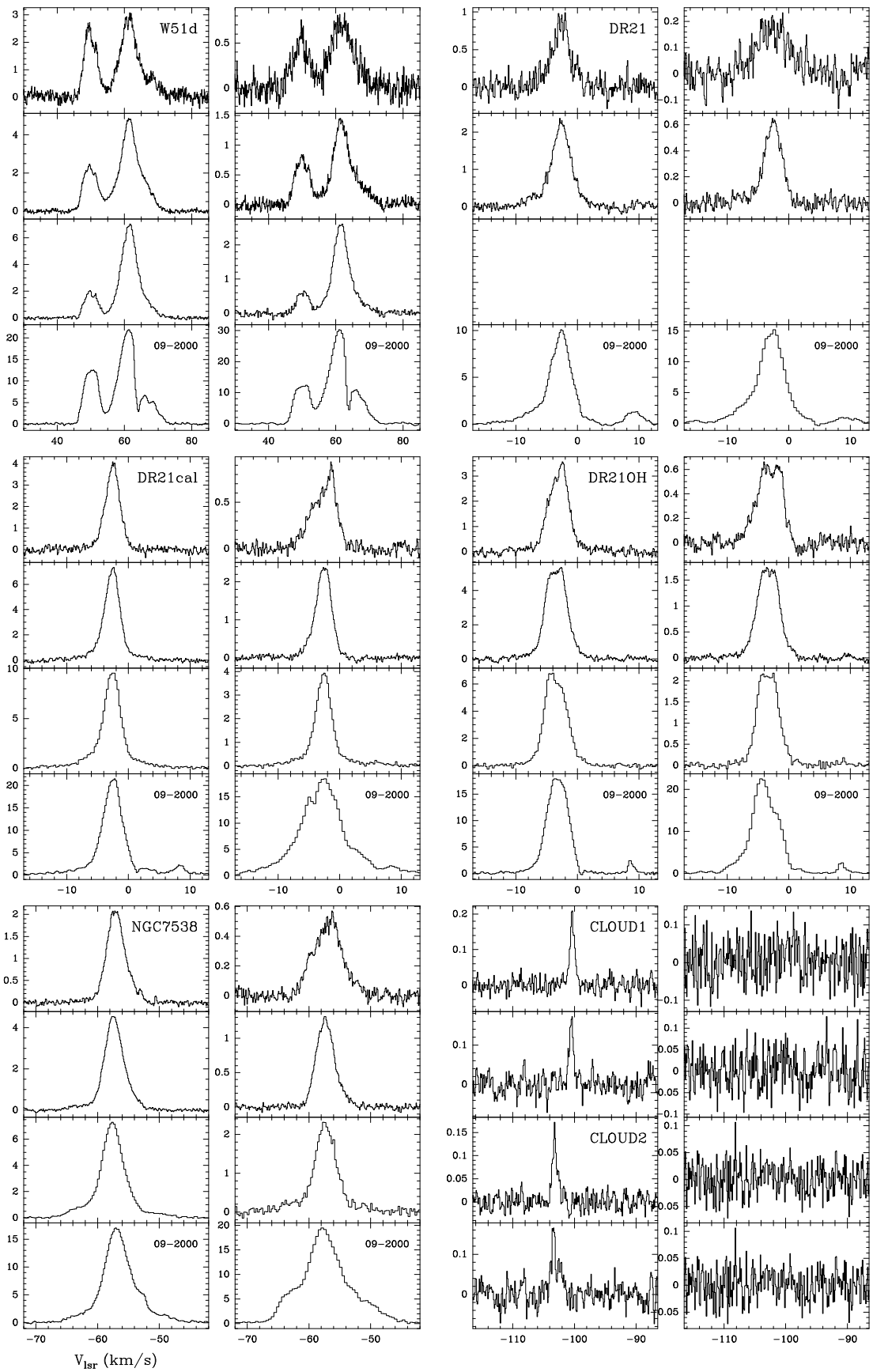


Fig. A.1. Continued. Towards DDT94 Cloud 1 and 2 only the $C^{18}O$ and $C^{17}O$ J=1–0 and 2–1 lines have been observed.